Indian Journal of Chemical Technology
Vol. 32, November 2025, pp. 723-733
DOI: 10.56042/ijct.v32i6.20285

Design and evaluation of eco-engineered B_4C/Fly ash composites: A green material for gamma and neutron shielding applications

Meryem Cansu Şahin[1]* & Kaan Manisa[2]

[1]Department of Medical Services and Techniques, Vocational School of Health Services, Usak University, Uşak Üniversitesi, 1 Eylül Kampüsü, Uşak, Türkiye

[2]Department of Physics, Faculty of Arts and Sciences, Kütahya Dumlupınar University, Kütahya, Türkiye

*E-mail: meryem.sahin@usak.edu.tr

Received 3 June 2025; accepted 6 October 2025

In this study, eco-engineered composite pellets made of fly ash and boron carbide (B_4C) are designed and evaluated for gamma-ray and neutron shielding applications. Composite samples with different B_4C ratios (0–75 wt%) have been prepared and examined using both theoretical and experimental methods. XRD and SEM are used for structural and morphological characterizations. A NaI(Tl) detector is used to measure gamma-ray attenuation parameters such as LAC, MAC, HVL, TVL, MFP, Z_{eff}, and buildup factors. These values are further evaluated using Phy-X/PSD and GAMOS simulations. Values for the fast neutron removal cross-section (FNRCS) are also calculated. The composite with the most balanced performance is BCFA25, which has a compact microstructure and improved attenuation efficiency. Increasing the content of boron and carbon with lower atomic numbers increased neutron shielding but decreased Z_{eff} and electron density. Strong agreement is found between theoretical models and experimental outcomes. The results indicate that B_4C/fly ash composites, especially BCFA25, offer a lead-free and sustainable option for radiation shielding in industrial, nuclear, and medical applications.

Keywords: B_4C, Fly ash, Gamma-ray shielding, GAMOS, Neutron shielding, Phy-X/PSD, Radiation shielding

Introduction

The increasing use of ionizing radiation in medical diagnostics, nuclear energy, space missions, and industrial applications has enlarged the need for effective and ecologically radiation shielding materials[1–3]. Conventional shielding materials like lead, though effective due to their high density and atomic number, causes serious health and environmental risks. Therefore, current research is focused on developing non-toxic, lightweight and cost-effective alternatives, especially those based on composite or ceramic systems[4–6].

Among advanced materials, boron carbide (B_4C) has gained prominence for its outstanding radiation attenuation capabilities, particularly for neutron shielding, owing to its high boron content and large neutron absorption cross-section[7]. Additionally, its low density (~2.52 g/cm^3)[8], excellent mechanical strength, and high-temperature stability make it suitable for portable and structural shielding applications[9]. The scientific literature has consistently demonstrated that the presence of boron and carbon atoms contributes to the observed moderate gamma-ray attenuation performance[10–13]. The incorporation of B_4C into composite formulations, encompassing polymers, concretes, and glasses, has been demonstrated to yield enhanced gamma and neutron attenuation characteristics[14–16].

Conversely, fly ash, a byproduct of coal combustion in industrial settings, is characterized by a high content of oxides, including SiO_2, Al_2O_3, Fe_2O_3, and CaO[17]. These components contribute to gamma-ray attenuation through mechanisms such as photoelectric absorption and Compton scattering, especially at lower photon energies[18–20]. The incorporation of fly ash into various construction materials, such as bricks, geopolymers, and concretes, has been studied for its potential to enhance shielding properties while concurrently reducing production costs and environmental impact [21–24].

In addition to fly ash, other industrial and mining waste products have been investigated for use in radiation shielding. For instance, Bi_2O_3-based waste composites, red mud, and heavy metal slag-derived materials have been reported to improve gamma-ray attenuation and contribute to sustainable waste management practices[25–27]. Incorporating references to these studies on waste-based shielding provides

broader context for situating the present work within the growing field of eco-friendly radiation shielding materials.

Although numerous studies have independently investigated the shielding capabilities of B_4C and fly ash in various matrices, there is no research on their combined use in a single composite system. In particular, the synergistic integration of B_4C and fly ash as hybrid shielding materials has not been extensively investigated, especially over a wide photon energy spectrum. This study evaluates the combined performance of the two materials and presents a new approach that takes advantage of the high neutron absorption capacity of B_4C with the cost-effectiveness and density of fly ash.

This study is based on the hypothesis that the synergistic incorporation of B_4C and fly ash at optimized ratios will yield eco-friendly composite materials with enhanced and well-balanced gamma-ray and neutron shielding capabilities, surpassing the performance achievable by either constituent material alone. Accordingly, the aim of this research is to evaluate the radiation shielding properties of B_4C/fly ash composites produced at different weight ratios. Both experimental measurements and theoretical approaches are employed to determine key gamma-ray attenuation parameters, including the linear attenuation coefficient (LAC), mass attenuation coefficient (MAC), half value layer (HVL), tenth value layer (TVL), mean free path (MFP), effective atomic number (Z_{eff}), electron density (N_{eff}), as well as buildup factors (EBF and EABF). To validate and complement the experimental findings obtained using a NaI(Tl) scintillation detector, calculations are performed with the Phy-X/PSD platform and Monte Carlo simulations. In addition, the fast neutron removal cross section (FNRCS) is determined to assess the neutron shielding performance of the composites.

Experimental Section

Materials preparation

Composite shielding pellets were prepared by mixing fly ash and B_4C in different weight ratios, where the proportions represent fly ash to B_4C by weight: 100:0, 75:25, 50:50, and 25:75. These composite materials were designated as BCFA0, BCFA25, BCFA50, and BCFA75, corresponding to the B_4C contents of 0 wt.%, 25 wt.%, 50 wt.%, and 75 wt.%, respectively. The B_4C powder (Nanografi Nano Teknoloji A.Ş., Ankara, Turkey) had 99.5% purity. Fly ash (Aker Kimya, İstanbul, Turkey) was sourced from a local thermal power plant. Each mixture was then compressed into cylindrical pellets using a uniaxial hydraulic press under 10 MPa pressure. The diameter, height, and mass of the cylindrical pellets were measured. Their volume was then calculated geometrically, and the measured mass was divided by the corresponding volume.

Characterization techniques

XRD analysis

For structural analysis, XRD measurements were conducted over a 2θ range of 10° to 90°, with a step size of 0.01° and a scan rate of 10°/min. The obtained diffraction patterns were analyzed using the Joint Committee on Powder Diffraction Standards (JCPDS) database for phase identification.

SEM analysis

SEM analysis (Phenom ProX equipped with a CeB6 gun) was used to observe the morphology, grain size, and distribution of B_4C and fly ash particles in the composite matrix. Prior to scanning, a thin gold layer (~8 nm) was deposited onto the surface of composites via sputter coating, thereby increasing surface conductivity. SEM analyses were performed at 15 kV to observe the morphology and evaluate the dispersion quality of the B_4C and fly ash in the composite. Backscattered electron images were captured at various magnifications to highlight compositional contrast.

Gamma-Ray Shielding Experiments

The gamma-ray attenuation characteristics of the pellets were investigated using a NaI(Tl) scintillation detector connected to a multichannel analyzer (MCA) (Fig. 1). The system was calibrated using certified gamma sources. To cover a wide photon energy, range from 81 keV to 1408 keV, standard gamma

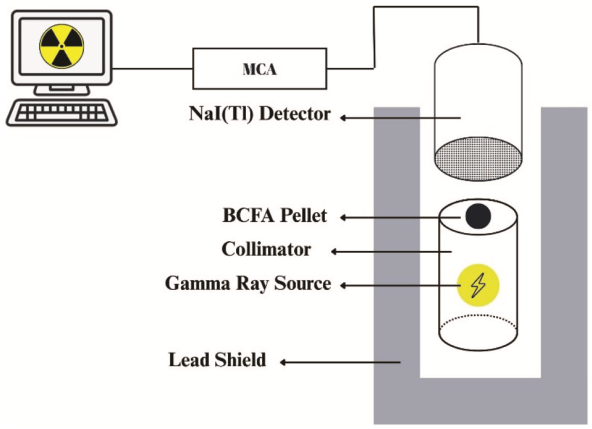

Fig. 1 — Scheme of experimental setup

sources including ^{133}Ba, ^{137}Cs, ^{59}Co, and ^{152}Eu were used. Each measurement was performed by placing the pellet between the source and the detector with a fixed geometry, and both incident (I_0) and transmitted (I) intensities were recorded. All measurements were repeated three times to ensure reproducibility.

The parameters under consideration for radiation shielding consist of the LAC, MAC, HVL, TVL, MFP Z_{eff} and N_{eff}. The formule for the parameters under consideration are provided below[28–33]:

$$\mathrm{LAC} = \frac{1}{x}\ln\left(\frac{I_0}{I}\right)$$

From LAC, the following shielding parameters were determined[34]:

$$MAC = \left[\frac{1}{x}\ln\left(\frac{I_0}{I}\right)\right]/\rho$$

$$HVL = \frac{ln2}{\mathrm{LAC}}$$

$$TVL = \frac{ln10}{\mathrm{LAC}}$$

$$MFP = \frac{1}{\mathrm{LAC}}$$

$$Z_{eff} = \frac{\sum_i f_i A_i \left(\frac{\mu}{\rho}\right)_i}{\sum_j f_j \frac{A_j}{Z_j}\left(\frac{\mu}{\rho}\right)_j}$$

$$N_{eff} = N_A \frac{N Z_{eff}}{\sum_i N_i A_i}$$

where I_0, I, x, ρ, and LAC are the incident radiation density, the transmitted radiation density, thickness of the composites, density of the composites and the linear attenuation coefficient, respectively.

Theoretical calculations

Phy-X/PSD Computation

In this study, Phy-X/PSD software was employed theoretically to calculate the gamma-ray attenuation parameters of the BCFA composite pellets[35]. Phy-X/PSD is a widely utilized, web-based computational platform specifically designed for evaluating photon interaction and dosimetric parameters across a broad energy spectrum. This tool was selected for its demonstrated capacity to accurately model fundamental photon interactions, such as the photoelectric effect, Compton scattering, and pair production, while simultaneously providing high computational reliability for materials of varying density, atomic number, and elemental composition.

The main advantage of Phy-X/PSD is its capacity to determine essential shielding parameters. These capabilities enabled a comprehensive theoretical evaluation of the gamma shielding efficiency of the composite materials developed in this work. For these reasons, it was selected as the primary tool for evaluating the photon attenuation behaviour of the BCFA composites in this work.

GAMOS simulations

To validate experimental results and evaluate photon interaction mechanisms, simulations were conducted using GAMOS[36]. In the theoretical part of this study, GAMOS v.6.2.0, a Monte Carlo simulation toolkit based on GEANT4, was employed to evaluate the gamma-ray attenuation properties of the BCFA composite pellets.

In the present work, the GAMOS simulation environment was configured to replicate the experimental setup used for gamma-ray attenuation measurements. The simulation geometry included a cylindrical NaI(Tl) scintillation detector, a collimator, and a BCFA composite pellet, all placed within an air-filled room of 200×200×200 cm³. The detector consisted of 2"×2" NaI(Tl) crystal, enclosed in aluminum housing with a metal light shield. The test sample was modeled as a cylindrical pellet and positioned along the central axis between the collimator and the detector[37].

A lead collimator was designed with a height of 10 cm, an outer diameter of 7 cm, and a 2 cm central aperture to produce a narrow photon beam directed toward the sample. The incident gamma-ray energies were defined to match those used in the experimental study, covering the range from 81 keV to 1408 keV.

The physics processes, source definitions, and dose scoring parameters were specified using the GAMOS input files. Electromagnetic physics modules were used to account for photoelectric absorption, Compton scattering, and pair production processes. Dose deposition in the NaI(Tl) crystal was recorded to determine the transmitted photon intensity. A total of 10^9 photon histories were simulated for each energy to ensure statistical reliability without applying variance reduction techniques.

Results and Discussion

The densities of BCFA0, BCFA25, BCFA50 and, BCFA75 composite materials are 2.6, 2.58, 2.55, 2.53 g/cm^3, respectively.

Structural and morphological characterization

The XRD patterns of the B_4C and fly ash are presented in Fig. 2. The boron carbide sample (Fig. 2a) predominantly shows peaks corresponding to boron carbide as referenced by JCPDS cards 01-071-0108; however, additional peaks associated with sodium aluminum silicate (JCPDS cards 01-072-1245) are also detected, suggesting the presence of minor impurities in the material. In the case of the fly ash sample (Fig. 2b), characteristic peaks of silicon oxide (JCPDS cards 01-078-1252) and aluminum silicon oxide (JCPDS cards 01-079-1454) were observed together.

The morphology and distribution of the composite components were examined through SEM analysis, as shown in Fig. 3. Each sample was imaged at ×5000 magnifications to assess dispersion and matrix integrity. B_4C and fly ash are clearly distinguishable in the micrographs. The images demonstrate that the B_4C and fly ash are well dispersed in matrix.

The BCFA0 composite (Fig. 3a) demonstrates a porous and irregular morphology, attributed to the absence of B_4C. Conversely, the incorporation of B_4C in the BCFA25 composite (Fig. 3b) results in a more compact structure, characterized by enhanced interparticle contact. As the B_4C content increased in BCFA50 and BCFA75 (Figs 3c and 3d), a more uniform and homogeneous particle distribution was observed. This is favourable for minimizing scattering losses and promoting consistent photon–matter

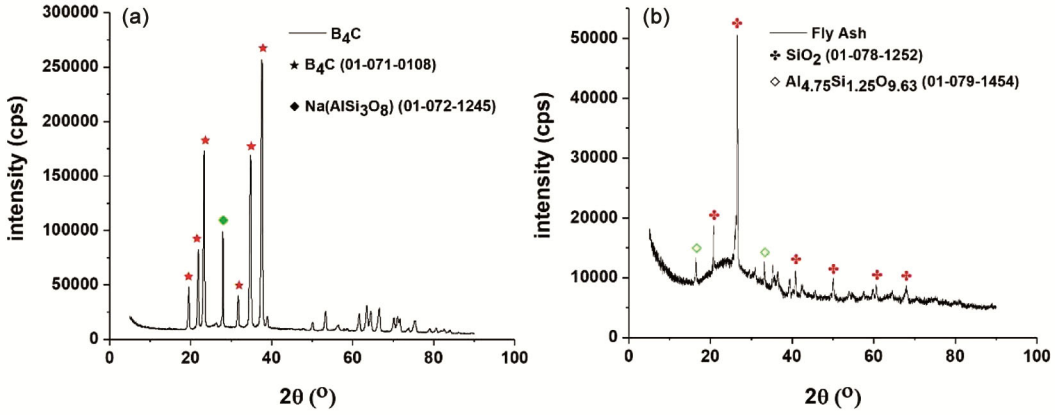

Fig. 2 — XRD patterns of (a) B_4C and (b) fly ash used in composite preparation

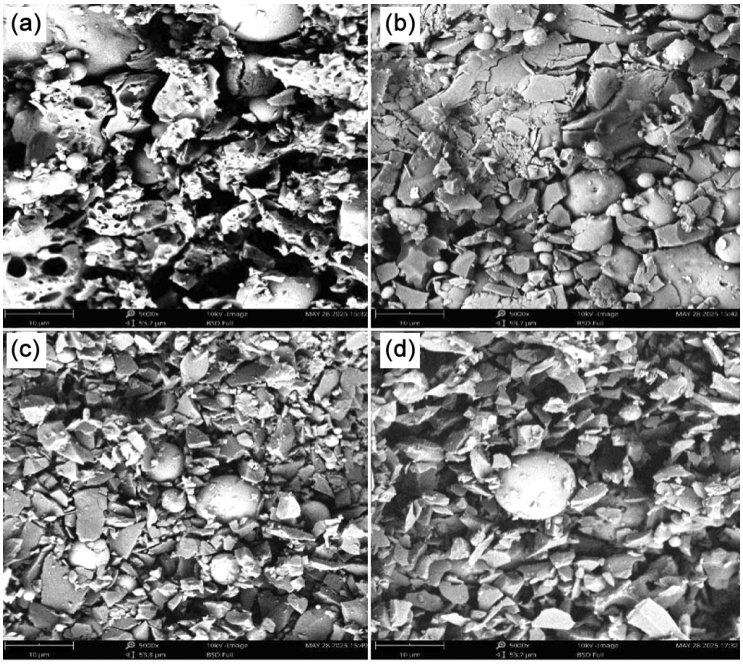

Fig. 3 — SEM images of (a) BCFA0, (b) BCFA25, (c) BCFA50 and (d) BCFA75 samples

interaction pathways. However, an excess of B_4C may result in reduced photon interaction parameters, such as the Z_{eff}. This underscores the advantage of a balanced composition in BCFA25.

Gamma-ray shielding parameters

The gamma-ray attenuation behaviour of the BCFA composite pellets was investigated across a wide energy spectrum ranging from 81 keV to 1408 keV. This investigation involved both experimental measurements and theoretical simulations. The shielding efficiency was quantified through the measurement of key parameters, including the LAC, MAC, HVL, TVL and, MFP.

A capacity of material to attenuate gamma radiation per unit thickness is primarily indicated by its LAC[38]. It is significantly influenced by the energy of the incident photons and the composite's physical properties, particularly its density and atomic composition. In the present study, LAC values for all BCFA composites demonstrated a consistent decline with increasing photon energy, which is typical for most shielding materials (Fig. 4). This phenomenon can be attributed to the changing dominance of gamma interaction mechanisms, in which photoelectric absorption is prominent at low energies, Compton scattering dominates at intermediate energies, and pair production becomes related at higher energies[10,39]. For example, at 81 keV, the LAC of BCFA50 was higher than that of BCFA75. This difference is due to the combined effects of the boron atoms, which increase interaction probabilities in the photoelectric region. As the energy increased to 662 keV and beyond, the differences between the samples became less distinct. This finding is consistent with the energy dependence of Compton scattering, which is relatively insensitive to atomic number but still affected by electron density[40]. Concrete and polymeric systems that have been previously studied have shown similar patterns, with higher LAC values being achieved at lower photon energies and a sharp decrease as energy increases[41,42]. The LAC values obtained through experimental means in this study demonstrated strong agreement with theoretical results derived from Phy-X/PSD and GAMOS. This finding serves to substantiate the reliability of the experimental and computational approaches that were employed in this study.

In competition, MAC, which normalizes the LAC by the density of material, provides deeper insight into the intrinsic photon interaction properties of the material regardless of its bulk mass[43]. Furthermore, the MAC values of the composites exhibited a decreasing trend with increasing photon energy, paralleling the changes observed in LAC (Fig. 5). The highest MAC values were recorded at lower energies, especially in BCFA25 and BCFA50, where B and O atoms played a critical role in enhancing photoelectric absorption. It is well-established that the photoelectric cross-section is proportional to approximately Z^4 to Z^5, making atomic number a critical factor at low energies[28,32]. As the energy of the photons increased, the MAC values stabilized due to the onset of Compton scattering, where the cross-section became more dependent on the electron density than on the atomic number[44]. This observation is in line with findings, which investigated fly ash and cementitious composites, and noted that fly ash-rich samples exhibit a sharper drop in MAC as energy increases,

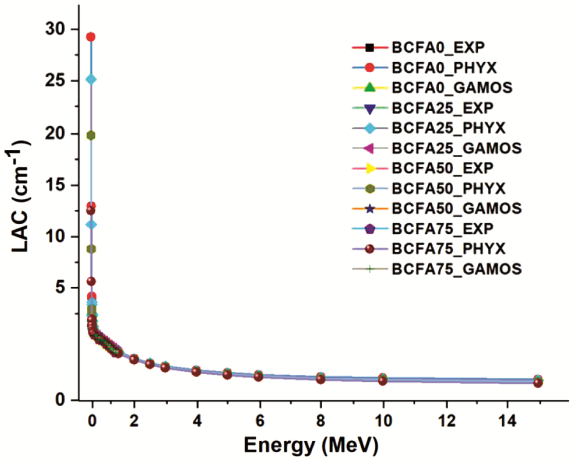

Fig. 4 — Experimental and theoretically obtained linear attenuation coefficient of BCFA composites

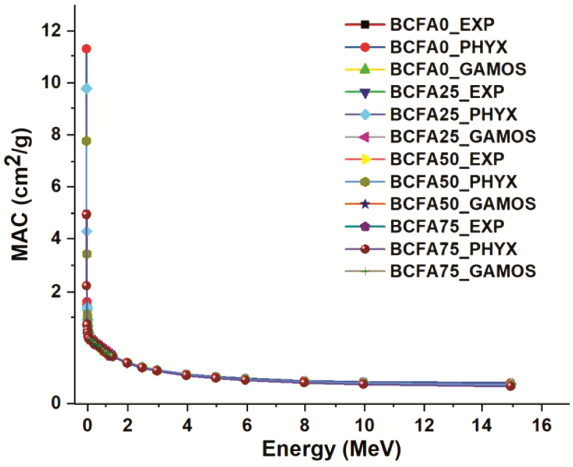

Fig. 5 — Experimental and theoretically obtained mass attenuation coefficient of BCFA composites

owing to their high Si and Al content, which are less effective at higher energies[19,45]. Furthermore, the relatively high MAC values in BCFA50 across all energy levels support the idea that an optimized BCFA ratio can maximize photon interaction efficiency while maintaining manageable composite density.

Among the fabricated composites, the BCFA25 sample exhibited the most balanced radiation shielding performance across the examined photon energy spectrum. This optimal behaviour is derived from the complementary characteristics of the two constituents: B_4C offers a high thermal neutron capture cross-section and moderate photon attenuation capacity[15,46], whereas fly ash, composed predominantly of mid-Z oxides such as SiO_2 and Al_2O_3, contributes significantly to gamma-ray interaction mechanisms, especially photoelectric absorption at low energies and Compton scattering at intermediate energies[22]. The resulting synergy enhances photon attenuation efficiency, which is indicated by the lower HVL and TVL values observed for BCFA25 (Fig. 6).

Another significant parameter employed to assess the shielding behaviour of the BCFA composites is MFP, which signifies the mean distance a gamma photon traveled in the material before undergoing an interaction[47]. MFP values are inversely proportional to the linear attenuation coefficient, meaning that materials with higher attenuation capabilities will exhibit shorter mean free paths[48]. In this study, MFP exhibited an increase with increasing photon energy, reflecting a decrease in the probability of photon-matter interaction at higher energies (Fig. 7). Among the samples that were examined, BCFA25 exhibited the lowest MFP values across a wide range of energy levels. This finding suggests that BCFA25 may possess a superior interaction efficiency and enhanced attenuation behaviour. It can be posited that the phenomenon under consideration is attributable to the optimized balance of B_4C and fly ash. The collective contribution of these elements to the creation of favourable atomic and electronic environments for interactions with photons has been demonstrated. The findings are consistent with prior reports in the literature, which have demonstrated that MFP values are effective comparative indicators for evaluating the shielding suitability of polymeric, ceramic, and industrial waste-based composites[49–51]. These findings further substantiate the conclusion that BCFA50 is a high-performance, structurally efficient composition for gamma-ray shielding.

Fig. 8 presents the variation of Z_{eff} and N_{eff} for the BCFA composite samples. Both parameters play significant roles in understanding the photon interaction behaviour and overall radiation attenuation performance of composite materials. Similar trends in

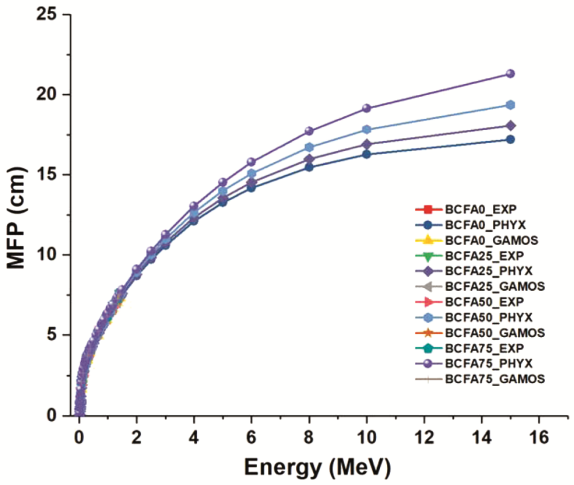

Fig. 7 — Mean free path of BCFA composites

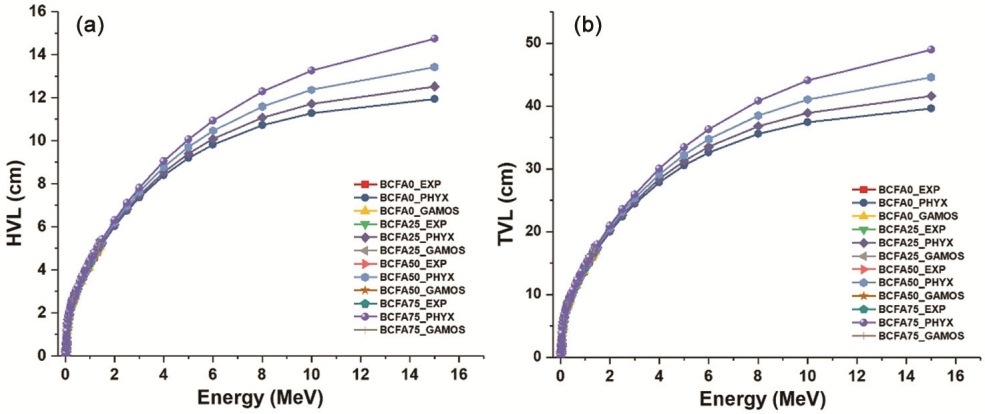

Fig. 6 — (a) HVL and (b) TVL values of BCFA composites as a function of photon energy

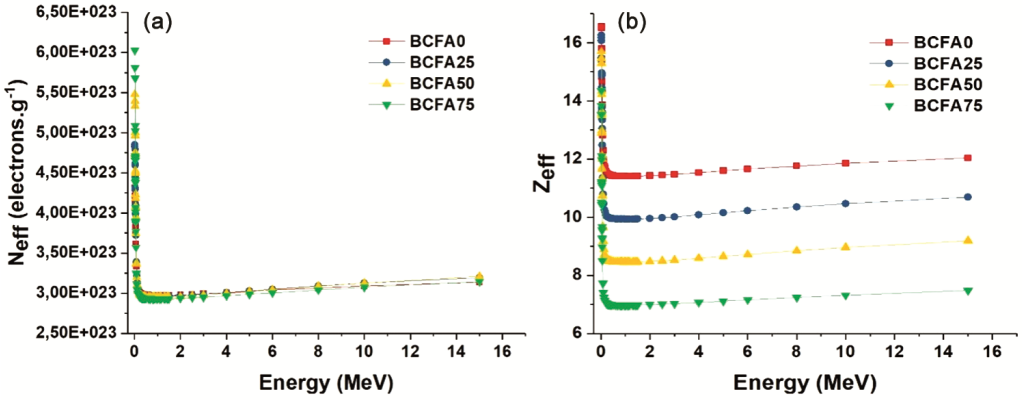

Fig. 8 — (a) N_{eff} and (b) Z_{eff} values of BCFA composites as a function of photon energy

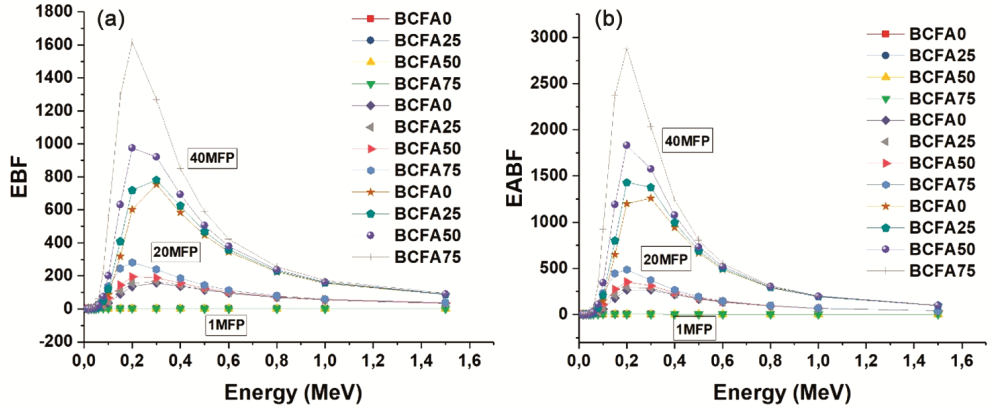

Fig. 9 — (a) EBF and (b) EABF values of BCFA composites at penetration depths of 1, 20, and 40 mean free paths

Z_{eff} density and composition have been reported in literature. This confirms that higher density and high-Z constituents consistently enhance photon interaction probabilities across different material systems[52,53].

The Z_{eff} values exhibit a sharp decline at lower photon energies, followed by a relatively stable region at higher energies. This energy-dependent behaviour reflects the dominance of different photon interaction mechanisms. At low energies, photoelectric absorption is predominant and highly sensitive to the atomic number, resulting in higher Z_{eff} values. As the energy increases, Compton scattering becomes the dominant interaction mechanism, which depends more on electron density than atomic number, thus stabilizing Z_{eff} values[54].

Among the composite samples, Z_{eff} decreases with increasing B_4C content. This trend can be attributed to the lower average atomic number of boron (Z = 5) and carbon (Z = 6) in B_4C compared to the heavier elements present in fly ash. Consequently, BCFA0 exhibits the highest Z_{eff} values across the entire energy range, whereas BCFA75 shows the lowest.

Similarly, N_{eff} also shows a declining trend with increasing B_4C content, as seen in Fig. 8. Electron density is influenced by both elemental composition and material density[55]. Since B_4C has a lower average electron density compared to the oxides in fly ash, its increasing presence leads to a reduction in the overall N_{eff} of the composite.

The variation of the EBF and EABF for the BCFA composite samples at different equivalent penetration depths (1, 20, and 40MFP) is illustrated in Fig. 9. Both EBF and EABF show a strong dependence on photon energy and penetration depth[56]. For all samples, a characteristic peak is observed in the intermediate energy region (around 0.3–0.4 MeV), which corresponds to the dominance of Compton scattering. Beyond this energy range, both EBF and EABF gradually decrease due to the increasing probability of pair production and the decreasing influence of multiple scattering[57].

As predicted, buildup factors exhibit an increase with penetration depth; values at 40 MFP are considerably higher than those at 1 MFP, suggesting a

greater contribution of scattered photons at deeper material layers. Among the compositions that were investigated, BCFA0 and BCFA25 consistently exhibited higher EBF and EABF values compared to BCFA50 and BCFA75. This phenomenon can be attributed to the increasing B_4C content in the composites, which has been demonstrated to enhance the photon attenuation capability and reduce the number of secondary photons contributing to buildup. On the other hand, fly ash, which contains a significant fraction of low-Z oxides, contributes less effectively to photon attenuation, resulting in higher buildup factors in composites with higher fly ash ratios.

The variation of the FNRCS for the composite shielding pellets is presented in Fig. 10. As observed, FNRCS values increase progressively with the increase in B_4C content in the composites. This behavior is attributed to the high neutron absorption capability of boron, which has a remarkably high neutron capture cross section for thermal and fast neutrons[58].

B_4C, being a boron-rich compound, serves as an effective neutron attenuating material due to its low atomic number and high neutron interaction probability. The rise in FNRCS values from BCFA0 to BCFA75 indicates that the neutron shielding efficiency of the composite is enhanced with higher B_4C concentrations. The obtained FNRCS values for the composites are in agreement with reported ranges for other waste-based shielding materials, where higher density and boron content were shown to enhance fast neutron removal capability[59,60]. As expected, the increase in B_4C content enhanced the FNRCS values, which can be attributed to the high neutron absorption cross section of boron. This trend

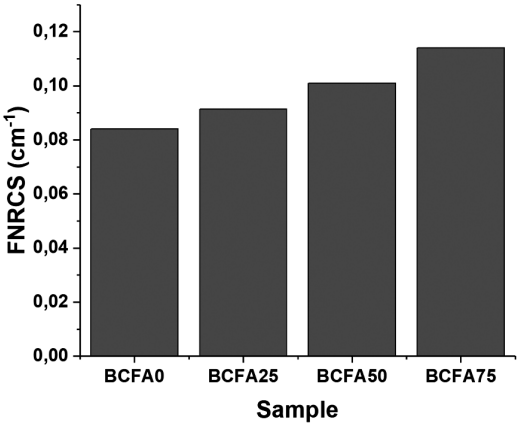

Fig. 10 — FNRCS values of BCFA composites

confirms that the neutron shielding performance of the composites is governed primarily by the B_4C ratio rather than the fly ash matrix. In contrast, fly ash mainly consists of oxides such as SiO_2 and Al_2O_3 which have relatively low neutron interaction cross sections. Therefore, composites with higher fly ash content exhibit lower FNRCS values. The improved FNRCS performance with increasing B_4C content confirms that B_4C acts as a dominant phase in neutron attenuation within the composite structure. This trend is consistent with the findings in previous studies that reported similar enhancements in neutron shielding with the incorporation of boron-based materials[61,62].

In addition to its notable effect on photon interaction parameters such as Z_{eff} and N_{eff}, B_4C also plays a crucial role in neutron attenuation, which is particularly significant in mixed radiation fields. Although increasing B_4C content leads to a slight reduction in Z_{eff} and N_{eff} due to the lower atomic number and electron density of boron and carbon, the overall shielding capability of the composites is enhanced when both photon and neutron attenuation are considered. This is because boron exhibits an exceptionally high thermal and fast neutron absorption cross section. Furthermore, the EBF and EABF demonstrated that higher B_4C content effectively suppresses photon scattering and secondary radiation generation. Therefore, the final analysis of FNRCS complements the previous findings by confirming the dual-functionality of B_4C as an efficient shielding material. While it moderately affects photon interaction characteristics, its dominant influence on neutron attenuation makes B_4C-containing composites highly suitable for applications where both gamma rays and neutrons are present.

Furthermore, to experimental evaluations, theoretical modeling was conducted using the Phy-X/PSD software and validated by Monte Carlo simulations through the GAMOS toolkit. The GAMOS toolkit replicates the full geometry of the experimental setup, including the NaI(Tl) detector, lead collimator, and sample geometry. The simulated LAC values exhibited a strong agreement with the experimental results, with relative errors generally below 10%, thereby affirming the accuracy and reliability of the experimental procedure. This agreement between theoretical predictions and measured data also validates the use of Phy-X and GAMOS in characterizing new radiation shielding materials[9].

Conclusion

The gamma-ray and neutron shielding capabilities of BCFA composite pellets were systematically examined in this study using both experimental and theoretical methodologies. The most balanced and efficient performance was demonstrated by BCFA25 among all compositions that were investigated. The specimen exhibited optimal linear and mass attenuation coefficients, as well as favourable half-value layer values, indicating superior attenuation with minimal material thickness. In addition, the uniform distribution of particles and relatively compact microstructure of BCFA25 led to a more consistent shielding behaviour and reduced photon scattering losses. As demonstrated by the FNRCS results, these findings suggest that the composites' fast neutron shielding efficacy is improved by increasing the B_4C content. Additionally, the suppression of accumulation effects is facilitated by higher B_4C ratios, which contribute to enhanced photon attenuation, particularly at higher energies and higher penetration depths. Therefore, it is imperative to optimize the B_4C-to-fly ash ratio in accordance with the specific radiation environment, whether it is characterized by a preponderance of neutrons, photons, or a combination of both. In conclusion, the BCFA25 composition exhibits significant potential as a promising candidate for lead-free, eco-friendly gamma-ray shielding applications. These composites are a prospective solution for use in medical, nuclear, and industrial environments where cost-effective radiation protection is important, as they integrate sustainability and performance through the incorporation of industrial by-products. Nevertheless, this study has certain limitations, such as the lack of mechanical, thermal, and long-term stability evaluations, as well as the restricted sample preparation route. To address these gaps, future research should extend the scope by investigating the structural durability of the composites under practical conditions, assessing large-scale manufacturing feasibility, and exploring the incorporation of additional eco-friendly reinforcing agents. Such efforts would provide a more comprehensive basis for the deployment of B_4C/fly ash composites in real-world radiation shielding applications.

Conflict of interest

The authors declare no conflict of interest.

References

1 Dridi W, Alsulami R A, Albarqi M M, Alsufyani S J & Hosni F, Radiation shielding features of Na_2O–P_2O_5 glasses doped with MnO experimentally and using FLUKA and Phy-X, *J Radiat Res Appl Sci*, 17 (2024) 100805.

2 Alzahrani J S, Alrowaili Z A, Mutuwong C, Olarinoye I O & Al-Buriahi M S, Radiation shielding competence of chalcogenide alloys with high Te content, *Appl Radiat Isot*, 196 (2023) 110759.

3 Dridi W, Daoudi M, Farah K & Hosni F, Monte Carlo validation of dose mapping for the Tunisian Gamma Irradiation Facility using the MCNP6 code, *Radiat Phys Chem*, 173 (2020) 108942.

4 Abualroos N J, Yaacob K A & Zainon R, Radiation attenuation effectiveness of polymer-based radiation shielding materials for gamma radiation, *Radiat Phys Chem*, 212 (2023) 111070.

5 Hermógenes G, Oliveira E B, Zambianchi J K & Zambianchi P, Development of lead-free materials for radiation shielding in medical settings: A Review, *J Biomed Phys Eng*, 186 (2024) 109521.

6 Tochaikul G, Tanadchangsaeng N, Panaksri A & Moonkum N, Eco-friendly and low-dose radiation shielding material using natural waste cuttlebone and silicone rubber composite, *Radiat Phys Chem*, 231 (2025) 112604.

7 Evans J A, DeHart M D, Weaver K D & Keiser D D, Burnable absorbers in nuclear reactors-A review, *Nucl Eng Des*, 391 (2022) 111726.

8 Perevislov S N, Shcherbak P V & Tomkovich M V, High density boron carbide ceramics, *Refract Ind Ceram*, 59 (2018) 32.

9 Sahin M C, Manisa K, Bircan H & Saygili S K, Experimental, theoretical, and biological investigations on radiation shielding parameters of boron-doped cerrobend alloys, *Revista Materia*, 29 (4) (2024), https://doi.org/10.1590/1517-7076-RMAT-2024-0366.

10 Dong M, Zhou S, Yang H & Xue X, Gamma ray attenuation behaviors and mechanism of boron rich slag/ epoxy resin shielding composites, *Nucl Eng Technol*, 55 (2023) 2613.

11 Biswas R, Sahadath H, Mollah A S & Huq M F, Calculation of gamma-ray attenuation parameters for locally developed shielding material: Polyboron, *J Radiat Res Appl Sci*, 9 (2016) 26.

12 Ekinci N, El-Agawany F I, Gurol A, Rammah Y S, Ahmed E M, Yılmaz D, Aygün B & Somer M, Physical properties, experimental and theoretical gamma-ray shielding properties of some boron compounds, *Radiat Phys Chem*, 194 (2022) 110012.

13 El-Agawany F I, Ekinci N, Mahmoud K A, Sarıtaş S, Aygün B, Ahmed E M & Ramma Y S, Gamma-ray shielding capacity of different B4C-Re-and Ni-based superalloys, *Eur Phys J Plus*, 136 (2021) 527.

14 Abdulrahman S T, Thomas S & Ahmad Z, Micro and nanostructured composite materials for neutron shielding applications, (Woodhead Publishing), (2020).

15 Thomas C, Rico J, Tamayo P, Setién J, Ballester F & Polanco J A, Neutron shielding concrete incorporating B4C and PVA fibers exposed to high temperatures, *J Build Eng*, 26 (2019) 100859.

16 Gheith A T, El-Sarraf M A, Hasan I E, Helal N L, Rizk R A, El-Sawy A A & El-Sayed A A, Assessment of a polymeric composite as a radiation attenuator and a restoration mortar for cracking in biological shields, *Nucl Phys At Energy*, 21 (2020) 361.

17 Abbass W, Ahmed M, Ahmed A, Aslam F, Aziz I & Alyousef R, Physio-chemical characterization of waste coal bottom Ash and coal fly Ash for potential use in the construction ındustry: A step towards waste elimination and a cleaner environment, Available at SSRN: https://ssrn.com/abstract=4487539 or http://dx.doi.org/10.2139/ssrn.4487539

18 Külekçi G, Investigation of fly ash added light concretes with respect to gamma radiation transmission properties of 133 Ba and 137 Cs, *Radiat Eff Defects Solids*, 176 (2021) 833.

19 Külekçi G, Investigation of gamma ray absorption levels of composites produced from copper mine tailings, fly ash, and brick dust, *J Mater Cycles Waste Manag*, 24 (2022) 1934.

20 Temuujin J, Surenjav E, Ruescher C H & Vahlbruch J, Processing and uses of fly ash addressing radioactivity (critical review), *Chemosphere*, 216 (2019) 866.

21 Frahat N B, Awed A S, Kassem S M, Abdel Maksoud M I A & Ibrahim O M O, Innovative shielding solutions by geopolymer paste and fly ash as effective substitution of cement materials for sustainable protection, *J Build Eng*, 87 (2024) 108977.

22 Catenacci M J, Luckarift H R, Friedman R J, Male A & Owens J R, Effect of fly ash composition and component quantities on the gamma radiation shielding properties of geopolymer, *Prog Nucl Energy*, 140 (2021) 103889.

23 Alzahrani J S, Alrowaili Z A, Olarinoye I O, Kırkbınar M, Çalışkan F & Al-Buriahi M S, Nuclear and radiation shielding performance of synthesized geopolymers with addition of CRT waste glass composites, *Radiat Phys Chem*, 233 (2025) 112706.

24 Alomayrah N, Alrowaili Z A, Arslan H, Olarinoye I O & Al-Buriahi M S, Silica-based geopolymers admixture of borosilicate waste glasses: A green material for gamma radiation shielding applications, *Ceram Int*, 50 (2024) 31966.

25 Alsafi K, El-Nahal M A, Al-Saleh W M, Almutairi H M, Abdel-Gawad E H & Elsafi M, Utilization of waste marble and Bi_2O_3-NPs as a sustainable replacement for lead materials for radiation shielding applications, *Ceramics*, 7 (2024) 639.

26 Al-Buriahi M S, Alomayrah N, Alsaiari N S, Tehçi T & Çalışkan F, Effect of Si_3N_4 on metakaolin clay-based geopolymers: EDS, SEM, hardness, and gamma radiation shielding properties, *Constr Build Mater*, 492 (2025) 142857.

27 Paulose R, Agrawal V, Arya R, Bijanu A, Rajak G, Nair P K, Mishra D, Khan M A, Bhisikar A, Singh U, Mondi P, Pendam J, Srivastava A K & Salammal S T, Red mud and bismuth oxide based X-ray shielding tiles for upcoming hospitals: A comprehensive study on phase quantification and physical properties, *Constr Build Mater*, 439 (2024) 137414.

28 Hubbell J, Photon cross sections, attenuation coefficients and energy absorption coefficients, *Natl Bur Stand Rep NSRDS-NBS29, Washingt DC*, (1969).

29 Berger M, Hubbell J, Seltzer S, Coursey J & Zucker D, XCOM: Photon cross section database, (1999).

30 Şahin M C & Manisa K, Evaluation of x-ray shielding ability of tungsten rubber: A GAMOS monte carlo study, *Süleyman Demirel Üniversitesi Fen Edeb Fakültesi Fen Derg*, 18 (2023) 1.

31 Şahin M C, Manisa K & Bircan H, Validation of a proposed equation for determining the half-thickness value of gamma and x-ray radiation, *Süleyman Demirel Üniversitesi Fen Edeb Fakültesi Fen Derg*, 18 (2023) 10.

32 Şahin M C, Kayhan M & Kayhan E, Assessment of radiation absorption parameters of lithium disilicate glass-ceramic used in dentistry: experimental and theoretical approaches, *J Aust Ceram Soc*, 61 (2025) 361.

33 Sahin M C, The impact of Li_2O concentration on mechanical and radiation attenuation properties of lithium zinc borotellurite glasses: an in silico study, *Indian J Phys*, 99 (2025) 2563.

34 Kayhan E, Şahin M C, Erdoğan T & Kayhan M, Electron and gamma-ray shielding performance of glass fiber-reinforced polyester composites with ınorganic fillers, *J Appl Polym Sci*, (2025) e57811.

35 Şakar E, Özpolat Ö F, Alım B, Sayyed M I & Kurudirek M, Phy-X/PSD: Development of a user friendly online software for calculation of parameters relevant to radiation shielding and dosimetry, *Radiat Phys Chem*, 166 (2020) 108496.

36 Arce P, Ignacio L J, Harkness L, Pérez-Astudillo D, Cañadas M, Rato P, de Prado M, Abreu Y, de Lorenzo G, Kolstein M & Díaz A, Gamos: A framework to do Geant 4 simulations in different physics fields with an user-friendly interface, *Nucl Instruments Methods Phys Res Sect A Accel Spectrometers: Detect Assoc Equip*, 735 (2014) 304.

37 Şahin M C, Kayhan M & Kayhan E, Investigation of the radiation absorption parameters of dental Yttria-stabilized zirconium dioxide, *J Aust Ceram Soc*, 61 (2025) 1613.

38 Echeweozo E O, Alomairy S, Alsaiari N S & Al-Buriahi M S, Effect of lead oxide addition on gamma radiation shielding properties of newly developed geopolymers: Theoretical and simulation studies, *Sci Rep*, 14 (2024) 29968.

39 Bichsel H & Schindler H, The Interaction of Radiation with Matter, *Particle Physics Reference Library*, (Springer International Publishing, Cham), (2020) 5.

40 Toker O, Bilmez B, Akçalı Ö, Özşahin Toker M & İçelli O, Practical simulation method for determination of effective atomic number from Rayleigh to Compton scattering ratio by MCNP, *Radiat Phys Chem*, 181 (2021) 109330.

41 Meng Q Y, Xu M X, Qu H T & Xie J J, Evaluation of photon shielding properties and exposure buildup factors for various clay using Geant4 simulation and Win XCOM, *J Radiat Res Appl Sci*, 18 (2025) 101409.

42 Gouda M M, Osman A F, Awad R & Badawi M S, Enhanced radiation shielding efficiency of polystyrene nanocomposites with tailored lead oxide nanoparticles, *Sci Rep*, 14 (2024) 19970.

43 Khattari Z Y, Afaneh F & Al-Omari S, Topological constraints-induced radiation shielding efficiency of SiO_2 α-cristobalite polymorphism: Signatures from Hirshfeld pseudo-surfaces, *Opt Mater*, 155 (2024) 115821.

44 Celik I C, Kamislioglu M, Yorulmaz N, Yasar M M & Durgun M, Case study of Er- and Dy-doped boron-aluminosilicate glasses on radiation shielding performance in the energy range 0.015–10 MeV with $MCNP_{6.2}$, *Radiat Phys Chem*, 218 (2024) 111551.

45 Mann H S, Brar G S, Mann K S & Mudahar G S, Experimental ınvestigation of clay fly ash bricks for gamma-ray shielding, *Nucl Eng Technol*, 48 (2016) 1230.

46 Sarkawi M S, Mohamed Z M R, Rabir M H, Idris F M & Zainal J, Radiation shielding properties of ferro-boron concrete, *IOP Conf Ser Mater Sci Eng*, 298 (2018) 012037.

47 Singh V P & Badiger N M, γ-ray interaction characteristics for some boron containing materials, *Vacuum*, 113 (2015) 24.

48 Shakeri J B & Biganeh A, Novel bisphenol a-based composite shields: Fast neutron and gamma attenuation by digital neutron-gamma discrimination, *Radiat Phys Chem*, 235 (2025) 112852.

49 Abdel-Maksoud M I A, Kassem S M, Ashour A H & Awed A S, Recycled high-density polyethylene plastic reinforced with ilmenite as a sustainable radiation shielding material, *RSC Adv*, 13 (2023) 20698.

50 El-Sawy A A, Heikal M, Ibrahim S M & Mohamed O A, Experimental and theoretical study on the physico-mechanical characteristics and radiation shielding capability of hardened alumina sludge waste-cement pastes containing $MnFe_2O_4$-nanoparticles, *Discov Appl Sci*, 6 (2024) 567.

51 El-Sharkawy R M, Abdou F S, Gizawy M A, Allam E A & Mahmoud M E, Bismuth oxide nanoparticles (Bi_2O_3 NPs) embedded into recycled- Poly(vinyl chloride) plastic sheets as a promising shielding material for gamma radiation, *Radiat Phys Chem*, 208 (2023) 110838.

52 Erdogan T, Eken S & Sahin M C, Theoretical investigation of radiation absorption properties of electrons, photons, and heavy ions in Fe-based shape memory biomedical alloys, *Radiat Eff Defects Solids*, (2025) 1.

53 Sahin M C, Erdogan T & Udristiou M T, Investigation of some radiation attenuation properties of biomedical magnesium alloys: A simulation-based study, *Radiat Eff Defects Solids*, (2025) 1.

54 Kumar A, Studies on effective atomic numbers and electron densities of nucleobases in DNA, *Radiat Phys Chem*, 127 (2016) 48.

55 Manohara S R, Hanagodimath S M, Thind K S & Gerward L, On the effective atomic number and electron density: A comprehensive set of formulas for all types of materials and energies above 1keV, *Nucl Instruments Methods Phys Res Sect B Beam Interact with Mater Atoms*, 266 (2008) 3906.

56 Singh H, Sharma J & Singh T, Extensive investigations of photon interaction properties for ZnxTe100-x alloys, *Nucl Eng Technol*, 50 (2018) 1364.

57 Kanani N S, Parekh D J, Vasoya N H, Pawar P P, Modi K B & More C V, Optimizing gamma radiation defence through strategic Fe3+ substitution in $CaCu_3Ti_4O_{12}$, *J Alloys Compd*, 1027 (2025) 180594.

58 Qi Z, Yang Z, Li J, Guo Y, Yang G, Yu Y & Zhang J, The advancement of neutron-shielding materials for the transportation and storage of spent nuclear fuel, *Materials*, 15 (2022) 3255.

59 Abdelmonem A M, Effect of BaO on some radiation shielding parameters of recycling waste soda lime silica glasses system, *Radiat Phys Chem*, 229 (2025) 112446.

60 Gaylan Y, Bozkurt A & Avar B, Investigating thermal and fast neutron shielding properties of B_4C, B_2O_3, Sm^2O_3, and Gd_2O_3 doped polymer matrix composites using monte carlo simulations, *Süleyman Demirel Üniversitesi Fen Edeb Fakültesi Fen Derg*, 16 (2021) 490.

61 Han J H, Seok S H, Jin Y H, Park J, Lee Y, Yeo H U, Back J H, Sim Y, Chae Y, Wang J, Oh G Y, Lee W, Park H, Bang I C, Kim J H & Kwon S Y, Robust 2D layered MXene matrix-boron carbide hybrid films for neutron radiation shielding, *Nat Commun*, 14 (2023) 6957.

62 Gu Y, Liu B, Yang Z, Wang S & Li M, Multiscale design and fabrication of neutron shielding fiber-reinforced composites Via boron-based polymer and layer-by-layer self-assembly of Go/B4c on carbon fiber surface, (2024).